

New Path-finding Method for Soft Particle Liquids

Qingqing Ma

November 25, 2014

Contents

0.1	Method	5
0.2	Results	9
0.2.1	Parameter Testing	9
0.2.2	Convergence of the Paths	10
0.2.3	$(\frac{\Delta R}{g})^2$	15
0.2.4	Participating Ratio	15
0.3	Comparison of Methods	17

List of Figures

1	Parameter test of δ_{di} of the new path finding method	10
2	Convergence of $(\frac{\Delta R}{g})^2$ with respect to ΔR with the new path finding method	11
3	Convergence of $(\frac{\Delta R}{g})^2$ with respect to ΔR with the original path finding method	12
4	Convergence of $(\frac{\Delta R}{g})^2$ with respect to N with the new path finding method	13
5	Convergence of $(\frac{\Delta R}{g})^2$ with respect to N with the original path finding method	14
6	Comparison of $(\frac{\Delta R}{g})^2$ with the new method and with the original method	15
7	Convergence of participation ratio $\frac{n}{N}$ with respect to N with the new path finding method	16
8	Comparison of participation ratio $\frac{n}{N}$ with the new method and with the original method	17

List of Tables

1	Comparison of computational performance of the new method and the original method.	18
---	--	----

List of Algorithms

1	New method of path finding for soft particle systems	9
---	--	---

0.1 Method

A new method of finding geodesics for soft particle liquids is given in this section. It follows the basic idea of the original method [1] based on Kuhn-Tucker theorem, that the path consists of segments of unconstrained steps ($V(\mathbf{R}) < E_L$) and segments of steps obeying the equality ($V(\mathbf{R}) = E_L$). Similar to the situation in the original method, the system always heads towards the end point until it hits an obstacle in the configuration space. The difference is how to form steps around the obstacles.

Given a pair of end points \mathbf{R}_i and \mathbf{R}_f , the landscape energy E_L is the bigger value of $V(\mathbf{R}_i)$ and $V(\mathbf{R}_f)$, $E_L = \max(V(\mathbf{R}_i), V(\mathbf{R}_f))$. The system has a configuration $\mathbf{R} = (\mathbf{r}_1, \dots, \mathbf{r}_j, \dots, \mathbf{r}_N)$ and a potential energy $V = V(\mathbf{R})$.

The path consists of direct steps and contour steps.

1. Direct Step

In direct step, the system always tries to go directly from its current position $\mathbf{R}(t)$ to the second end point \mathbf{R}_f , with a small step size δ_{di} . This part is the same as in the original method in Chapter 3. Direct steps form the segments of free propagation of a path based on Kuhn-Tucker theorem.

$$\mathbf{R}^0(t+1) = \mathbf{R}(t) + \delta_{di} \frac{\mathbf{R}_f - \mathbf{R}(t)}{|\mathbf{R}_f - \mathbf{R}(t)|} \quad (1)$$

In calculation $\delta_{di} = 0.001\sigma$ is used.

If the trial position $\mathbf{R}^0(t+1)$ is in the allowed region of configuration space ($V(\mathbf{R}^0(t+1)) < E_L$), it is accepted as the next position.

1)) $\leq E_L$), this $\mathbf{R}^0(t+1)$ is accepted as the new configuration of the system along the path. The system will proceed from there.

2. Contour Step

If the trial position is in a forbidden region of configuration space ($V(\mathbf{R}^0(t+1)) > E_L$), the system first retreats to its position $\mathbf{R}(t)$ before the failed direct step. The system then takes a contour step. (Similar to the case of hard sphere method in Chapter 3, the hard sphere system first retreats to its last allowed position before the failed direct step, then takes a collision avoidance step.)

Denote the $3N$ dimensional gradient vector of potential energy function $V(\mathbf{R})$ as $\nabla V(\mathbf{R})$.

The level set Φ of potential energy function V at an arbitrary configuration $\mathbf{R}(t)$ is

$$\Phi(\mathbf{R}(t)) = \{\mathbf{R} : V(\mathbf{R}) = V(\mathbf{R}(t))\} \quad (2)$$

The gradient of V at $\mathbf{R}(t)$ is perpendicular to the level set of V at $\mathbf{R}(t)$.

$$\nabla V(\mathbf{R}(t)) \perp \Phi(\mathbf{R}(t)) \quad (3)$$

Denote the unit vector pointing from the current position of the system $\mathbf{R}(t)$ to the second end point \mathbf{R}_f as $\hat{\mathbf{d}}$.

$$\hat{\mathbf{d}} = \frac{\mathbf{R}_f - \mathbf{R}(t)}{|\mathbf{R}_f - \mathbf{R}(t)|} \quad (4)$$

$\hat{\mathbf{d}}$ can be decomposed to two perpendicular vectors \mathbf{f} and \mathbf{g} , with \mathbf{f} perpendicular to ∇V and \mathbf{g} parallel to ∇V . \mathbf{g} is the projection of $\hat{\mathbf{d}}$ along the direction of

∇V , and \mathbf{f} is $\hat{\mathbf{d}} - \mathbf{g}$.

$$\hat{\mathbf{d}} = \mathbf{f} + \mathbf{g} \quad (5)$$

$$\mathbf{g} = \frac{\hat{\mathbf{d}} \cdot \nabla V}{|\nabla V|} \frac{\nabla V}{|\nabla V|} \quad (6)$$

$$\mathbf{f} = \hat{\mathbf{d}} - \mathbf{g} \quad (7)$$

$$\mathbf{g} \parallel \nabla V, \quad \mathbf{g} \perp \Phi(\mathbf{R}(t)) \quad (8)$$

$$\mathbf{f} \perp \nabla V, \quad \mathbf{f} \parallel \Phi(\mathbf{R}(t)) \quad (9)$$

$$\mathbf{f} \perp \mathbf{g} \quad (10)$$

Since $\mathbf{f} \perp \nabla V$, if the system moves along the direction \mathbf{f} , the move does not increase the potential energy V . We can move the system according to

$$\mathbf{R}^0(t+1) = \mathbf{R}(t) + \delta_{di} \hat{\mathbf{f}} \quad (11)$$

$$\hat{\mathbf{f}} = \frac{\mathbf{f}}{|\mathbf{f}|} \quad (12)$$

$$\delta_{di} = 0.001\sigma \quad (13)$$

Contour steps form the segments of a path that satisfy the constraints as equality based on Kuhn-Tucker theorem.

Equation 11 does not increase the potential energy of the system in principle. Due to numerical precision in calculation, in some cases the move may need a

small component in the direction of $-\mathbf{g}$ to decrease the potential energy a little bit. An iteration is used to deal with this situation.

$$\mathbf{R}^n(t+1) = \mathbf{R}(t) + \delta_{di}\hat{\mathbf{f}} - \delta_c^n \frac{\nabla V}{|\nabla V|} \quad (14)$$

$$\delta_c^n = 10^{-5}n\sigma \quad (15)$$

where $n = 0, 1, 2, \dots, n_{max}$ is the index of iteration. The iteration stops when $V(\mathbf{R}^n(t+1)) \leq E_L$. In most cases, no iteration is needed and $n_{max} = 0$. In some cases two or three iterations are needed. (In the original method in Chapter 3 a tolerance δV is used to deal with numerical error, which serves the same purpose.) The configuration $\mathbf{R}^{n_{max}}(t+1)$ is accepted as the new configuration of the system along the path. The system proceeds from there.

3. A path is found when the distance between the current configuration of the system $\mathbf{R}(t)$ and the second end point \mathbf{R}_f is smaller than δ_{di} .

$$|\mathbf{R}_f - \mathbf{R}(t)| < \delta_{di} \quad (16)$$

The path length l is the sum of the lengths of every successful step (steps connecting two consecutive allowed configurations) along the path.

$$l = \sum_{t=0}^{t=P} |\mathbf{R}(t+1) - \mathbf{R}(t)| \quad (17)$$

where P is the total number of steps along the path, $\mathbf{R}(0) = \mathbf{R}_i$, $\mathbf{R}(P+1) = \mathbf{R}_f$.

This method is shown in Algorithm 1.

Algorithm 1 New method of path finding for soft particle systems

```
 $E_L \leftarrow \text{MAX}(V(\mathbf{R}_i), V(\mathbf{R}_f))$   
 $l \leftarrow 0$  ▷ path length  
 $\mathbf{R}_t$  ▷ current configuration of the system  
 $\mathbf{R}_o$  ▷ previous allowed configuration of the system  
 $\mathbf{R}_t \leftarrow \mathbf{R}_i, \mathbf{R}_o \leftarrow \mathbf{R}_i$   
while  $|\mathbf{R}_f - \mathbf{R}_t| > \delta_{di}$  do ▷  $\delta_{di} = 0.001\sigma$   
   $\mathbf{R}_o \leftarrow \mathbf{R}_t$   
   $\mathbf{R}_t \leftarrow \mathbf{R}_t + \delta_{di} \frac{\mathbf{R}_f - \mathbf{R}_t}{|\mathbf{R}_f - \mathbf{R}_t|}$  ▷ direct step  
  if  $V(\mathbf{R}_t) > E_L$  then  
     $\mathbf{R}_t \leftarrow \text{CONTOURSTEP}(\mathbf{R}_o)$  ▷ contour step  
  end if  
 $l \leftarrow l + |\mathbf{R}_t - \mathbf{R}_o|$   
end while  
return  $l$ 
```

procedure CONTOURSTEP(\mathbf{R}_o)

```
   $\mathbf{R}$   
   $\delta_c \leftarrow 0$   
   $\hat{\mathbf{d}} \leftarrow \frac{\mathbf{R}_f - \mathbf{R}_o}{|\mathbf{R}_f - \mathbf{R}_o|}$   
   $\hat{\nabla}V \leftarrow \frac{\nabla V}{|\nabla V|}$   
  repeat  
     $\mathbf{R} \leftarrow \mathbf{R}_o + \delta_{di} \frac{\hat{\mathbf{d}} - (\hat{\mathbf{d}} \cdot \hat{\nabla}V)\hat{\nabla}V}{|\hat{\mathbf{d}} - (\hat{\mathbf{d}} \cdot \hat{\nabla}V)\hat{\nabla}V|} - \delta_c \hat{\nabla}V$  ▷  $\delta_{di} = 0.001\sigma$   
     $\delta_c \leftarrow \delta_c + 10^{-5}\sigma$   
  until  $V(\mathbf{R}) \leq E_L$   
  return  $\mathbf{R}$   
end procedure
```

0.2 Results

The procedure of setting up molecular dynamics and finding pairs of end points is the same as in Chapter 3.

0.2.1 Parameter Testing

The step size $\delta_{di} = 0.001\sigma$ is used throughout the calculations with the new method.

Fig. 1 shows the convergence of $(\frac{\Delta R}{g})^2$ with respect to the parameter δ_{di} .

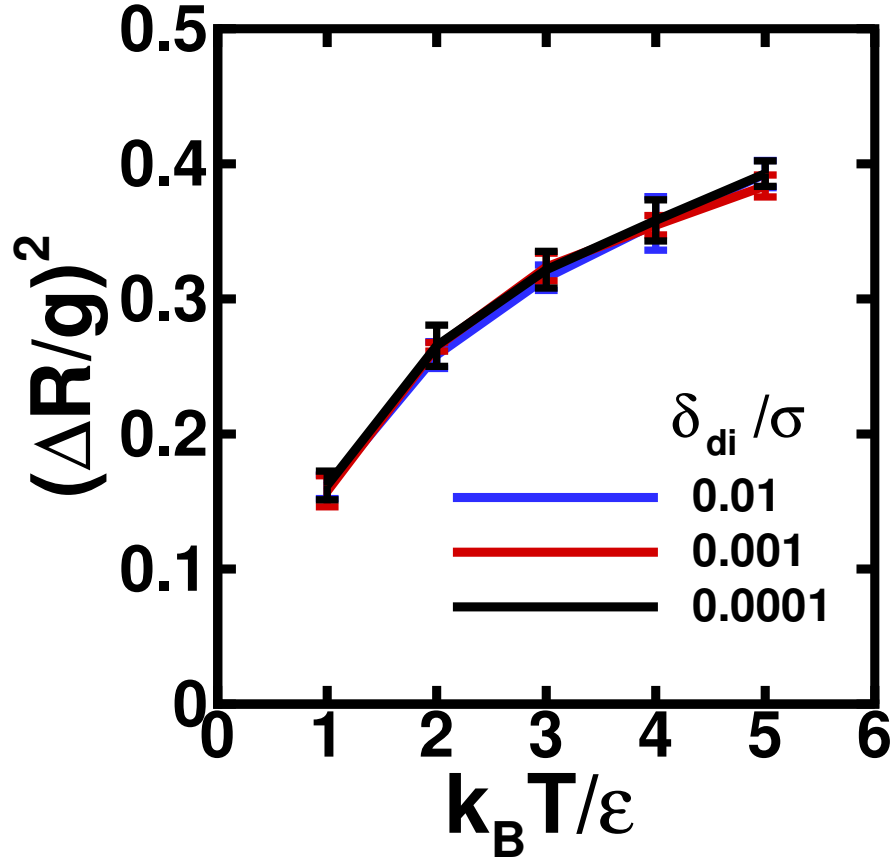


Figure 1: Parameter test of δ_{di} of the new path finding method. The system is Kob-Andersen liquid of size $N = 108$. The reduced temperature $k_B T/\epsilon$ decreases from 5.0 to 1.0. The results are averaged over 5 unoptimized paths of $\Delta R = 108\sigma$.

Fig. 1 shows that the path lengths generated with the three different tested values of the parameter δ_{di} are numerically very close. Computationally the time t needed to find a path is $t(\delta_{di} = 0.01\sigma) < t(\delta_{di} = 0.001\sigma) < t(\delta_{di} = 0.0001\sigma)$. Because in the original method $\delta_{di} = 0.001\sigma$ is used as the direct step length, here $\delta_{di} = 0.001\sigma$ is chosen.

0.2.2 Convergence of the Paths

Fig. 2 shows the convergence of $(\frac{\Delta R}{g})^2$ with respect to ΔR with the new path finding method. Fig. 3 shows the convergence of $(\frac{\Delta R}{g})^2$ with respect to ΔR with the original path finding method. Comparing the graphs, the new method has similar convergence

rates to the original method with respect to ΔR .

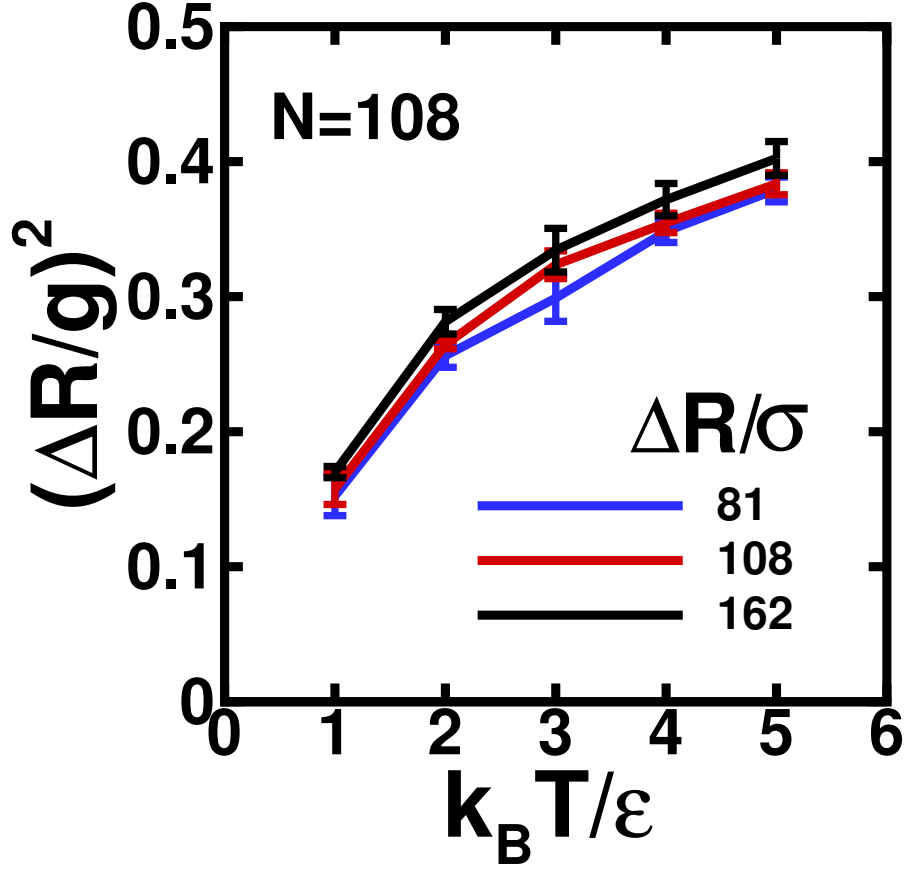


Figure 2: Convergence of $(\frac{\Delta R}{g})^2$ with respect to ΔR with the new path finding method. The system is Kob-Andersen liquid of size $N = 108$. The reduced temperature $k_B T/\epsilon$ decreases from 5.0 to 1.0. The results are averaged over 5 unoptimized paths. The figure shows that $(\frac{\Delta R}{g})^2$ is converged with ΔR within fluctuation.

Fig. 4 shows the convergence of $(\frac{\Delta R}{g})^2$ with respect to N with the new path finding method. Fig. 5 shows the convergence of $(\frac{\Delta R}{g})^2$ with respect to N with the original path finding method. Comparing the graphs, the new method has similar convergence rates to the original method with respect to N .

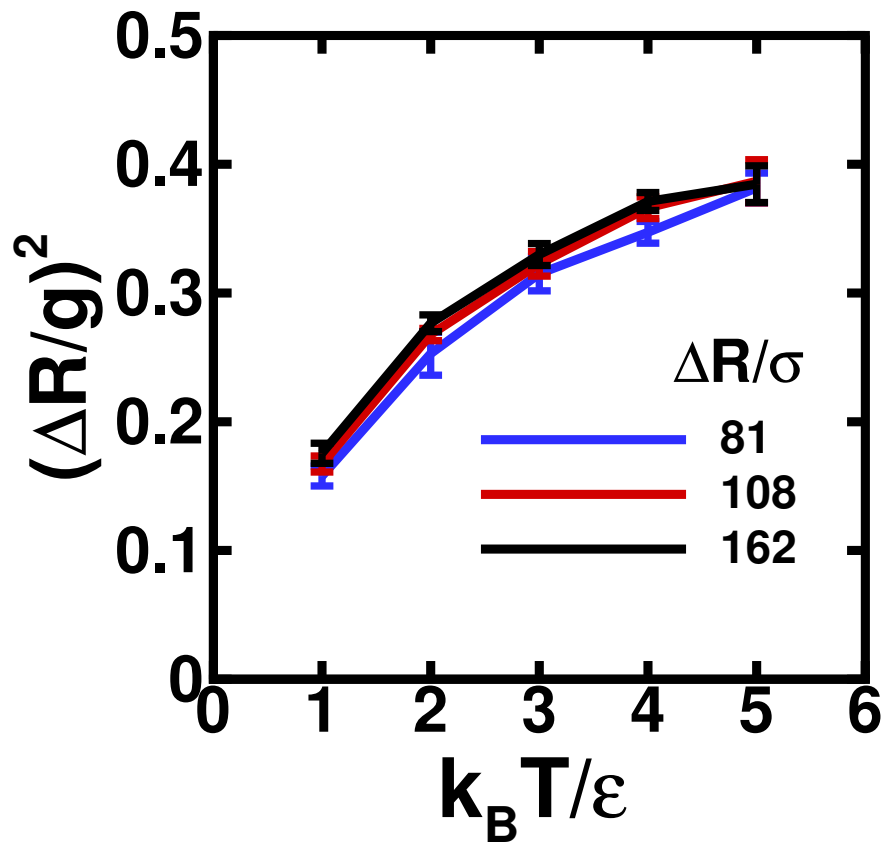


Figure 3: Convergence of $(\frac{\Delta R}{g})^2$ with respect to ΔR with the original path finding method. The system is Kob-Andersen liquid of size $N = 108$. The reduced temperature $k_B T/\epsilon$ decreases from 5.0 to 1.0. The results are averaged over 5 unoptimized paths. The figure shows that $(\frac{\Delta R}{g})^2$ is converged with ΔR within fluctuation.

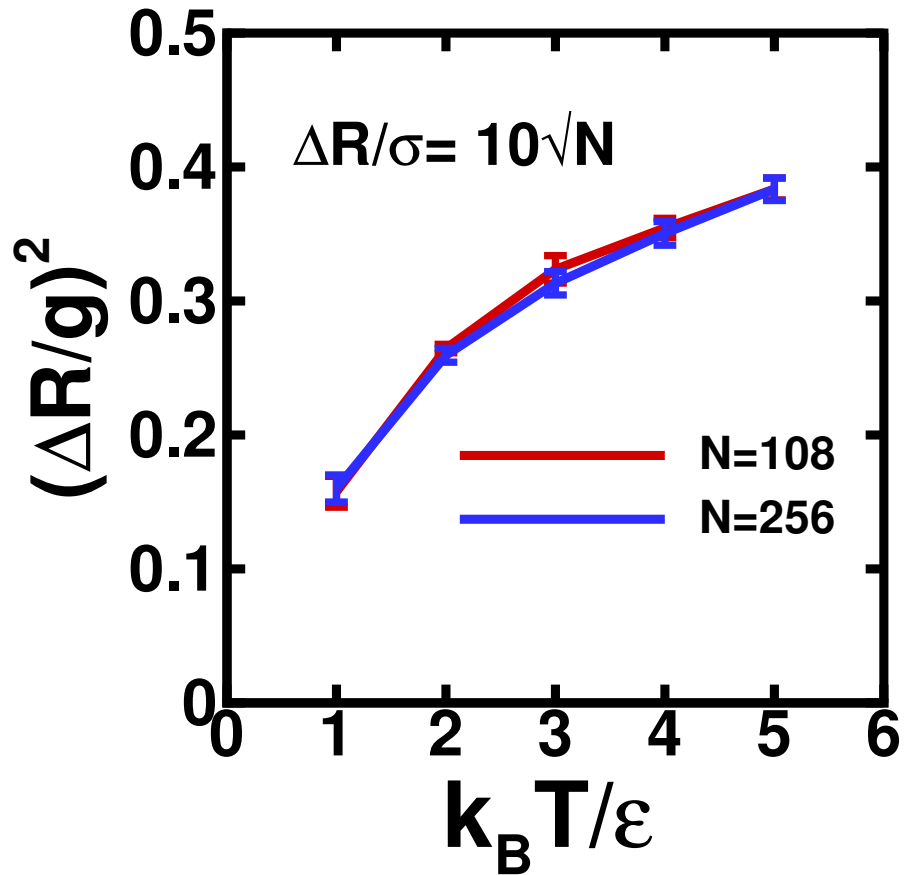


Figure 4: Convergence of $(\frac{\Delta R}{g})^2$ with respect to N with the new path finding method. The system is Kob-Andersen liquid of sizes $N = 108$ and $N = 256$. The reduced temperature $k_B T/\epsilon$ decreases from 5.0 to 1.0. The results are averaged over 5 unoptimized paths. The figure shows that $(\frac{\Delta R}{g})^2$ is converged with N within fluctuation.

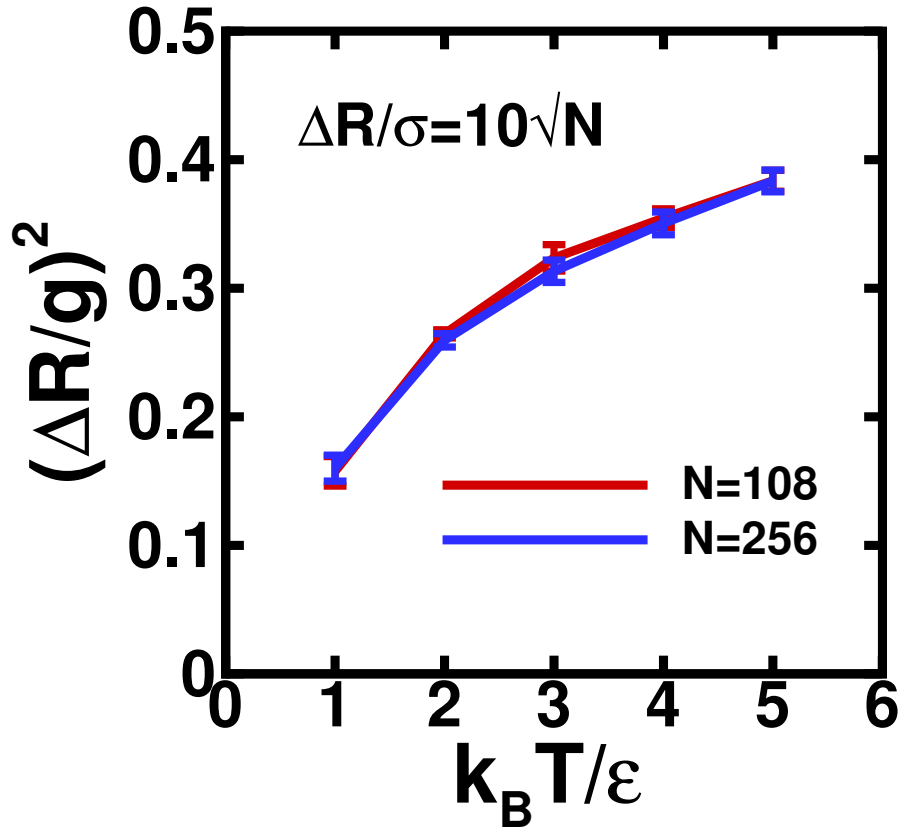


Figure 5: Convergence of $(\frac{\Delta R}{g})^2$ with respect to N with the original path finding method. The system is Kob-Andersen liquid of sizes $N = 108$ and $N = 256$. The reduced temperature $k_B T / \epsilon$ decreases from 5.0 to 1.0. The results are averaged over 5 unoptimized paths. The figure shows that $(\frac{\Delta R}{g})^2$ is converged with N within fluctuation.

0.2.3 $(\frac{\Delta R}{g})^2$

Fig. 6 shows the comparison of $(\frac{\Delta R}{g})^2$ with the new method and with the original method.

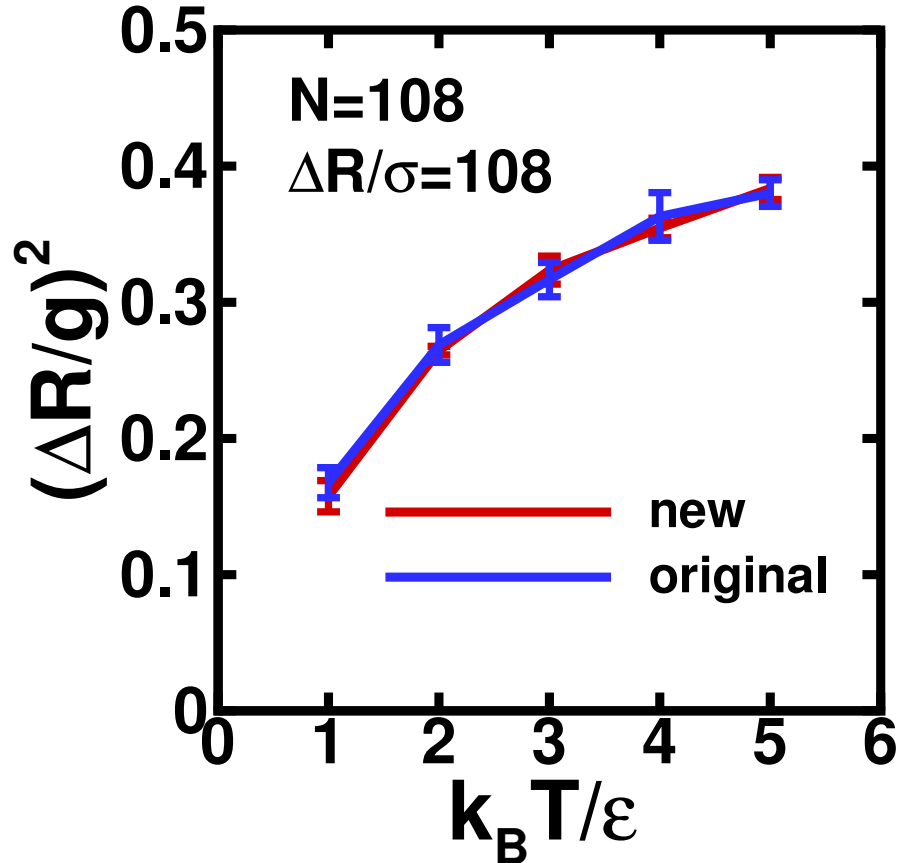


Figure 6: Comparison of $(\frac{\Delta R}{g})^2$ with the new method and with the original method. The system is Kob-Andersen liquid of size $N = 108$. The reduced temperature $k_B T/\epsilon$ decreases from 5.0 to 1.0. The results of both methods are averaged over 5 unoptimized paths of $\Delta R = 108\sigma$. The figure shows that the two methods give close numerical results for $(\frac{\Delta R}{g})^2$.

0.2.4 Participating Ratio

Fig. 7 shows the convergence of participation ratio n/N with respect to N with the new path finding method.

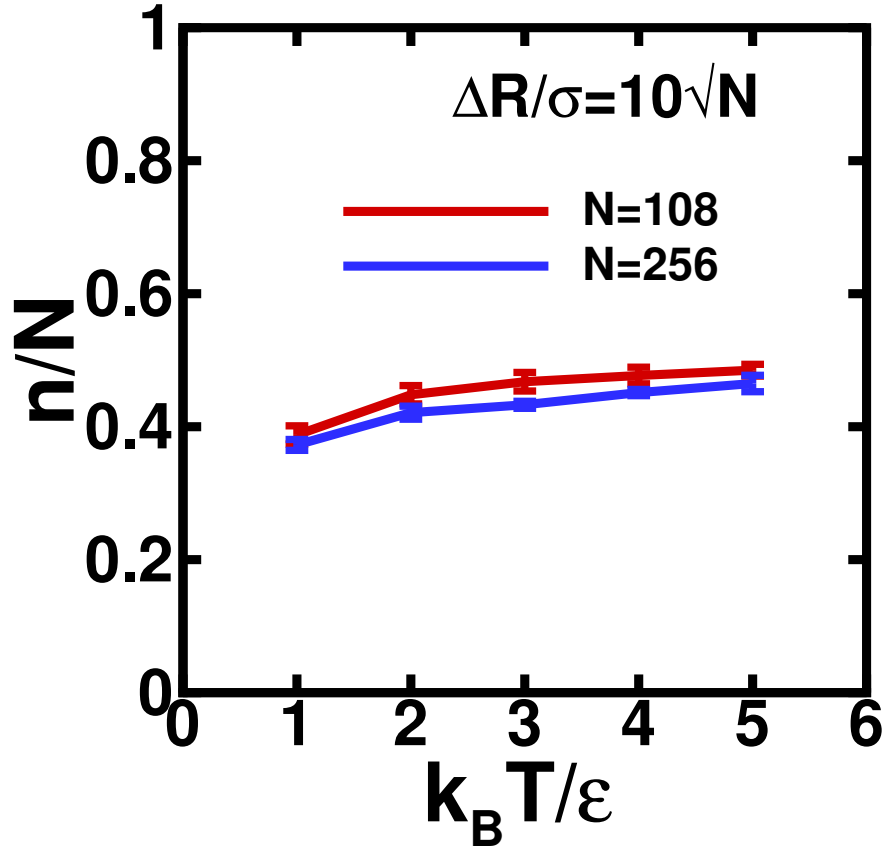


Figure 7: Convergence of the participation ratio n/N with respect to N with the new path finding method for the Kob-Andersen liquid. The reduced temperature $k_B T / \epsilon$ decreases from 5.0 to 1.0. The results are averaged over 5 unoptimized paths. The figure shows that n/N is converged with N within fluctuation. The motions along the paths are therefore macroscopic.

Fig. 8 shows the comparison of participation ratio $\frac{n}{N}$ with the new method and with the original method.

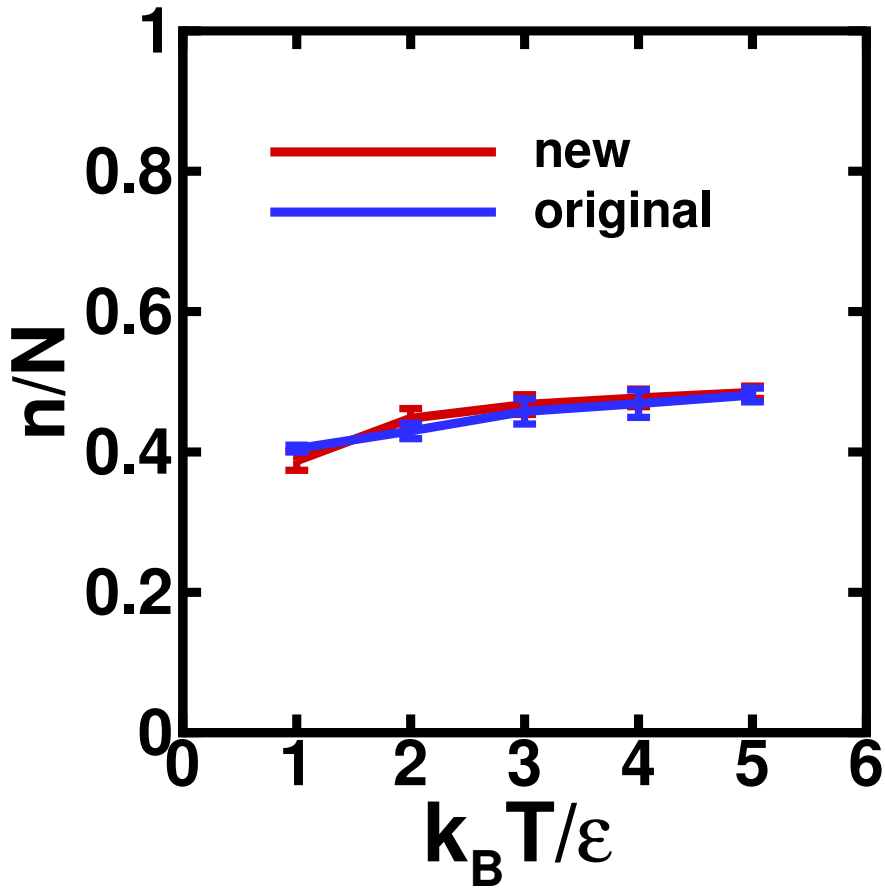


Figure 8: Comparison of participation ratio n/N with the new method and with the original method for the Kob-Andersen liquid. The reduced temperature $k_B T / \epsilon$ decreases from 5.0 to 1.0. The results of both methods are averaged over 5 unoptimized paths of $N = 108$ and $\Delta R = 108\sigma$. The figure shows that the two methods give close numerical results of $\frac{n}{N}$.

0.3 Comparison of Methods

All the above figures show that the new method is able to generate converged paths, and the results are numerically very close to those of the original method. The two methods are both based on Kuhn-Tucker theorem, with the difference in implementing the segments of paths that obey the constraints as equality. The contour step in the new method, as the counterpart of the escape step in the original method, allows the system to move along the boundary too. The system does retreat to the allowed configuration first before the contour step, and that configuration does not usually lie

exactly on the boundary. But as long as the step length is small, the configuration is still very close to the boundary, so is the contour step.

In the escape step in the original method, iteration is needed in the gradient descend method to find the nearest allowed configuration from the disallowed trial location. In the new method, no such iteration is needed. This saves computational time because it does not have to compute the potential energy multiple times for one step. We compare the computational performance of the two methods in Table 1. The time listed in the table is the rough average amount of time needed for a method to find a path, given a pair of end points, averaged over 5 unoptimized paths of $N = 108$ and $\Delta R = 108\sigma$ for Kob-Andersen liquid. The table shows that the efficiency of the new method is about 10 times higher than the original method.

$k_B T/\epsilon$	time(seconds) - new method	time(seconds) - original method
5.0	750	12000
4.0	800	12000
3.0	850	12000
2.0	900	13000
1.0	1100	15000

Table 1: Comparison of computational performance of the new method and the original method. The table lists the time needed to find a path for both methods. Both results are averaged from 5 unoptimized paths of $N = 108$ and $\Delta R = 108\sigma$ for Kob-Andersen liquid. The new method consumes about one tenth of the time of the original method to find a path.

Another advantage of the new method is that, if the nearest allowed configuration \mathbf{R} where the escape step in the original method takes the system to happens to have the property that $\hat{\mathbf{d}}$ is perpendicular to $\nabla V(\mathbf{R})$, the next direct step would take the system back to the forbidden region, then the following escape step would take the system back to the same nearest allowed point \mathbf{R} again. The program would stay in an infinite loop. The new method, on the other hand, does not have this problem.

Bibliography

- [1] Chengju Wang and Richard M Stratt. Global perspectives on the energy landscapes of liquids, supercooled liquids, and glassy systems: geodesic pathways through the potential energy landscape. *The Journal of Chemical Physics*, 127(22):224504, December 2007.